Dewetting dynamics of ultrathin silver films on Si(111)

K. Thürmer,[1,*] E. D. Williams,[1,2] and J. E. Reutt-Robey[3,†]
[1]*Department of Physics, University of Maryland, College Park, Maryland 20742-4111, USA*
[2]*Institute for Physical Science and Technology, University of Maryland, College Park, Maryland 20742-4111, USA*
[3]*Department of Chemistry and Biochemistry, University of Maryland, College Park, Maryland 20742-4111, USA*
(Received 10 March 2003; revised manuscript received 30 May 2003; published 23 October 2003)

Continuous silver films of nanometer thickness, grown at room temperature on (7×7)-Si(111), display a wormlike morphology and thermally decay into isolated three-dimensional crystallites. We have tracked the dewetting process in real time using variable-temperature scanning tunneling microscopy. In this ultrathin regime, a range of transitional morphologies are observed, dependent on the substrate step density, annealing time and temperature. Initial film morphology is modulated by the underlying step structure and the growing crystallites show a corresponding step-induced deformation. During the initial stages of dewetting, the Ag-denuded areas transform to the $(\sqrt{3}\times\sqrt{3})R30°$-Ag/Si(111) surface, and spatially nonuniform denuded zones appear around the growing crystallites. Enhanced dewetting rates are observed in areas of lower step density, largely because steps act as kinetic obstacles. A simple form to relate the energy gain in dewetting to the density of crystallographic steps is provided. On preprepared $(\sqrt{3}\times\sqrt{3})R30°$-Ag/Si(111) substrates, dewetting occurs spontaneously even at room temperature.

DOI: 10.1103/PhysRevB.68.155423 PACS number(s): 68.37.Ef, 68.55.Jk, 68.60.Dv

I. INTRODUCTION

Thin solid films have an ever-expanding range of applications in electronic devices, chemical sensors, and catalysts. A basic understanding of the stability of these films is vital to these applications. Wetting properties of thin solid films are particularly significant, as the long-term stability of the films, and the potential for forming self-assembling two-dimensional film patterning, is subject to thermally activated changes in film structure and continuity. Given the number of publications devoted to thin film growth, the literature concerning solid film stability is relatively scant. This is surprising because the majority of heteroepitaxial systems, i.e., films grown on a foreign substrate, energetically favor island growth and thus are subject to capillarity or dewetting instability. In practice, ultrathin continuous films are produced at low temperatures, where reduced diffusion suppresses transport of the film material into three-dimensional 3(D) islands.

An earlier study by Jiran and Thompson[1] addressed the dewetting dynamics of 30–90-nm thick gold films on fused silica. Using a combination of electron microscopy and optical transmission measurements, the authors reported a liquidlike behavior. The recession of the continuous edge of the dewetting film appears unaffected by basic structural elements such as film grain boundaries or substrate steps at the micron-length scale of observation. More recently, dewetting studies of soft films[2] have focused on the influence of film thickness (10–100-nm range) on dewetting instabilities. These studies generally assume a smooth substrate and neglect crystalline aspects of dewetting. In contrast to these earlier studies, we explore *crystalline* aspects of solid dewetting. By selecting extremely thin (1 nm) films and low annealing temperatures, we operate in a regime where the crystalline microstructure becomes dominant. The application of scanning tunneling microscopy (STM) under ultrahigh vacuum conditions allows resolution of key structural elements, such as crystallographic steps, on both the substrate and film.

For the present experiments, we select Ag/Si(111) as our model system. The growth properties of silver on Si(111) have been studied extensively, providing excellent background for our dewetting experiments. This heteroepitaxial system can be easily prepared and investigated in UHV: Silver deposited at room temperature onto (7×7)-Si(111) develops an almost continuous film already at $\approx$4 atomic layers mean film thickness.[3–5] Further advantages of the Ag/Si(111) system are the convenient onset temperature for dewetting $T\approx200-250\,°C$ (Ref. 6) and the absence of silicide formation. The very small intrinsic mechanical film stress with a zero-crossing at 0.5 nm (Ref. 7) can be neglected as a driving force. According to reflection high-energy electron-diffraction observations[9] and intrinsic stress measurements,[7] silver films grown at room temperature on Si(111) exhibit negligible strain. Hence the dewetting process described in this paper is driven by surface energies.

Under thermal activation, Aburano *et al.*[8] found that the Ag/Si(111) interface transforms into a bulklike 1×1 structure with intermixing confined to one atomic layer. The $\sqrt{3}\times\sqrt{3}$ reconstruction nucleates at step edges and grows outward onto the intervening terraces.[9,10] The $(\sqrt{3}\times\sqrt{3})$ surface further supports very high diffusion rates for Ag adatoms.[11,12]

II. EXPERIMENTAL PROCEDURES

Initial surfaces are created by room temperature deposition of 1-nm Ag onto two distinct substrates: (7×7)-Si(111) and $(\sqrt{3}\times\sqrt{3})R30°$-Ag/Si(111). The Ag/Si samples were then transferred (under ultrahigh vacuum) to the STM for time-lapsed measurements of the dewetting process. During these STM measurements the samples were annealed on the STM stage by resistive heating. The substrates were cut from highly doped 0.01-Ω cm Si wafers to permit

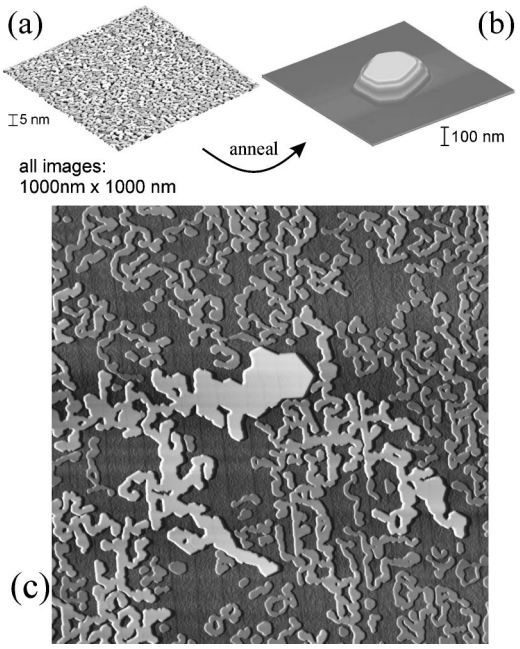

FIG. 1. (a) STM image of a 1-nm-thick Ag film deposited at room temperature onto (7×7)-Si(111). This film is metastable and transforms upon annealing for 4 h at $T=350\,^{\circ}\mathrm{C}$ into (b) a state closer to equilibrium, consisting of supported three-dimensional crystallites. (c) STM snapshot of a transitional morphology acquired after 2 h of annealing at 350 °C.

fine adjustment of the annealing temperature in the range of interest. However, the absolute sample temperature is rather inaccurate ($\pm50\,^{\circ}\mathrm{C}$), because sample temperature on the STM stage is extrapolated from a calibration based on pyrometer measurements conducted at considerably higher temperatures.

III. RESULTS AND DISCUSSION

The dewetting process for Ag/(7×7)-Si(111) causes a dramatic change in film structure, as shown in Fig. 1. Initially, deposition of a 1-nm-thick silver film on a room temperature (7×7)-Si(111) substrate produces a continuous metastable silver film [Fig. 1(a)] with a characteristic wormlike morphology with atomically flat Ag(111) termination. The typical width of the branches of the wormlike structures is 10 nm. The wormlike structures are separated by grain boundary grooves of ~1-nm depth. Ultimately, the imbalance in the specific free enthalpies, $\Delta\sigma=\sigma_{\mathrm{film}}+\sigma_{\mathrm{interface}}-\sigma_{\mathrm{substrate}}>0$, drives the system into the energetically favorable configuration characterized by larger isolated 3D crystallites [Fig. 1(b)]. We tracked the transformation between these two states in real-time using a variable temperature STM. A typical transitional morphology is captured in Fig. 1(c).

The transitional morphologies are highly sensitive to annealing temperature. Figures 2(a)–2(d) show snapshots from four different experimental runs with differing annealing protocols. All images represent a comparable stage of agglomeration in which ≈20% of the surface area is in the $\sqrt{3}\times\sqrt{3}$ reconstruction, with the remaining ≈80% surface area covered by the silver film. There is a clear trend from compact (circa 20-nm diameter) shapes produced by a longer anneal at the lowest temperatures [Fig. 2(a)] towards very elongated spaghettilike shapes with characteristic lengths $\gg$100 nm produced by shorter anneals at the higher temperatures [Fig. 2(d)]. These spaghetti-like features have comparable widths to the worms, but height variations that are increased by a factor of three. For the time-lapsed studies, described below, we focused on the intermediate cases, depicted in Figs. 2(b) and 2(c), where dewetting proceeds at a convenient time scale for STM investigation.

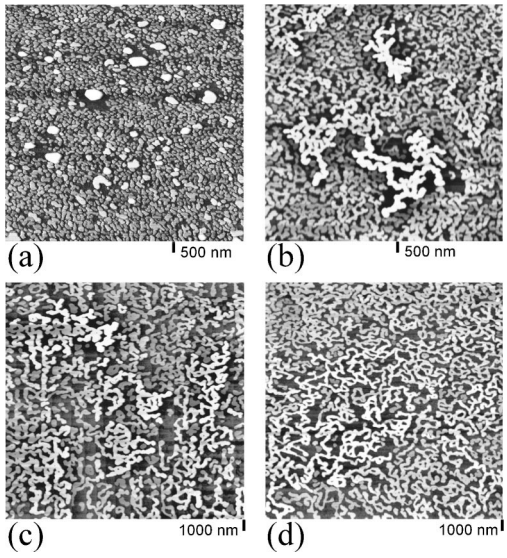

FIG. 2. Variety of transitional shapes as a result of different annealing protocols. (a) 2 h at 200 °C+2 h at 250 °C. (b) 1 h at 275 °C. (c) 2 h at 200 °C+0.5 h at 300 °C. (d) 0.5 h at 350 °C.

The time evolution of such a dewetting event is tracked with the time-lapsed STM images of Fig. 3. Figure 3(a) shows the initial surface for the dewetting experiments, prior to annealing. In agreement with the spot-profile analysis low energy electron diffraction (SPA-LEED) study by Moresco *et al.*[5] we find that the grain boundary grooves between the wormlike structures already extend to the substrate at some points, such as those marked with arrows. Thus the nucleation stage[1,13] of dewetting, during which holes penetrating the entire film must be formed, is eliminated for these single-nm films. In this regime, there is a subtle preference for grain boundaries to align along substrate steps which run vertically in Fig. 3. The weak vertical patterning in the film matches the periodicity of the underlying step structure. (The average substrate terrace width is 50 nm, and the step down direction is to the right.)

Upon raising the sample temperature to 350 °C, the dewetting process is thermally activated, as shown in the subsequent STM images of Figs. 3(b)–3(j). At early times, film material migrates to the top of existing wormlike structures increasing their height but preserving their irregular shape [Fig. 3(b)]. The inset in Fig. 3(b) illustrates that the freshly exposed patches of substrate area exhibit already the characteristic two-atomic-level pattern[14] of the $(\sqrt{3}\times\sqrt{3})R30°$-Ag/Si(111) reconstruction.[15,16] After 70–80 min

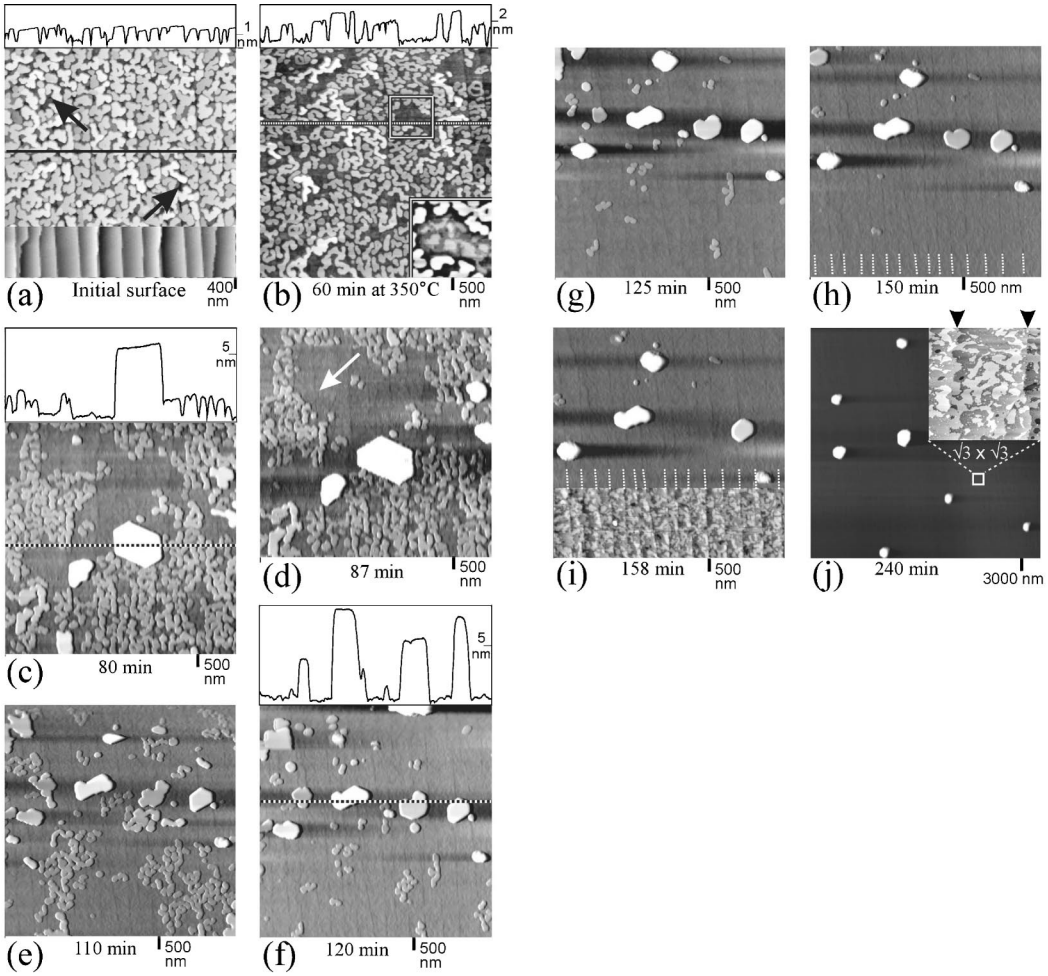

FIG. 3. (a) Composite image shows (7×7)-Si(111) surface before (image bottom) and after (image top) room temperature deposition of 1-nm Ag film. The predeposition image is dominated by step-edge contours. In the as-deposited image, silver worms faintly trace step edges. Topographic profile of the as-deposited film along line is inset above. (b)–(j) Time sequence of STM images taken during a dewetting experiment at $T=350\,^{\circ}\mathrm{C}$. Topographic profiles are provided for the transitional morphologies in panels (b), (c), and (f). The substrate step down direction is from left to right. Inset in (b): The denuded patch [marked by a rectangle in (b)] is enlarged, grayscale-adjusted and presented as a lower-right inset in (b). This inset shows the two-level pattern that serves as the signature of the $\sqrt{3}\times\sqrt{3}$ reconstruction. (h) and (i) Dotted vertical lines mark positions of the original Si-substrate steps. (i) At the image bottom the grayscale in a crystallite-free region has been adjusted to reveal the irregular two-level pattern of the $\sqrt{3}\times\sqrt{3}$ substrate. (j) Late-stage image with inset showing $\sqrt{3}\times\sqrt{3}$-substrate topography. Arrows mark predeposition substrate step positions.

at 350 °C, 3–5-nm-high hexagonal crystallites with atomically flat (111) top facets emerge [Fig. 3(c)]. The dissolution of the wormlike structures, which feed these emerging crystallites, is not uniform: Rather, the wormlike structures dissolve in patches, such as the 100×100-nm^2 denuded zone indicated by the arrow in Fig. 3(d). This suggests that the formation of the $\sqrt{3}\times\sqrt{3}$-Ag reconstruction on the denuded areas generates a positive feedback for dewetting, in which the vastly increased diffusion[11,12] of Ag atoms on the $\sqrt{3}\times\sqrt{3}$ surface accelerates the decay of adjacent worm structures.

The anisotropy of the formation of the denuded zone also impacts the growth shape of the crystallite. As shown in Figs. 3(c) and 3(d) the lower left edge of the large crystallite advances while other edges remain static, even though they are much closer to the remaining wormlike structures. Effective release of material from the wormlike structures evidently depends on the local structure produced by a previous step in the dewetting process, presumably the formation of the $\sqrt{3}\times\sqrt{3}$ structure in the immediate denuded area. As this heterogeneous system evolves, and the crystallites become surrounded by denuded areas, the remaining worms [Figs. 3(e)–3(h)] demonstrate no obvious order for consumption by larger crystallites. At the later stages of dewetting, after 125 min at 350 °C [Fig. 3(g)], some of the initial worm structures persist. It is likely that these structures are stabilized by a surrounding area which has not yet undergone the $\sqrt{3}\times\sqrt{3}$ reconstruction. The pattern of the root-three substrate morphology between the growing crystallites is illustrated in the inset to Fig. 3(j).

After the last worm-like features have disappeared (and the $\sqrt{3}\times\sqrt{3}$ reconstruction is complete) the surface continues

to transform via conventional Ostwald ripening. The late-stage surface, imaged after four hours at temperature and shown in Fig. 3(j), is decorated with large silver crystallites (circa 500 nm wide and up to 100 nm high) separated by the $\sqrt{3}\times\sqrt{3}$-reconstructed surface.

In contrast to liquidlike dewetting,[1,2] dewetting of Ag on Si(111) is sensitive to variations in local morphology. In this ultrathin regime, we have found that the density of crystallographic steps on the silicon substrate has a strong influence on the dewetting process. To study this effect further, we conducted experiments on regions of the silicon surface with a shallow curvature (i.e., variable step density) that resulted from imperfect crystal polishing. On such surfaces, a 1-nm-thick Ag film was annealed at $T=300\,^{\circ}\mathrm{C}$ for 450 min to achieve a partial dewetting, and the sample was then quenched to room temperature to preserve the dewetting state of the film. Film structure was then determined for areas of varied substrate step densities. One such region of shallow curvature is depicted in Figs. 4(a)–4(c). Near the center of this ''dimple'' was a relatively flat region, labeled *f*, with very large $L=100$ nm wide terraces. Along the perimeter of this dimple, labeled *d* and *e*, were regions with much narrower terraces. Since the original Si-substrate steps are not discernable in these higher-step-density areas we deduced the average terrace width from the local tilt of the surface measured by STM. A 200-nm-wide terrace [center of Fig. 4(d)] serves as the reference (111) plane (tilt$=0°$). By zooming into the areas labeled *d*, *e* and *f*, respectively, we can compare the dewetting for different substrate terrace widths under otherwise exactly identical conditions. The trend that larger terraces facilitate dewetting is very striking: For an average terrace width $L=12.5$ nm dewetting has merely begun [Fig. 4(d)], whereas for $L=100$ nm the agglomeration is already complete [Fig. 4(f)].

We next consider possible factors that could make dewetting rates sensitive to step density. One thermodynamic possibility involves elastic strain energy. Figure 3(a) reveals that the original worm structures tend to avoid the substrate steps. The crystallites that are produced by dewetting do, however, cross substrate steps as shown in Fig. 5. Since the step heights for Si(111) and Ag(111) are different $\Delta h=h_{\mathrm{Si}}-h_{\mathrm{Ag}}=3.135\ \text{Å}-2.36\ \text{Å}=0.77\ \text{Å}$, crystals extending over several substrate terraces are necessarily bent by a substrate step. This elastic deformation can be seen directly in the STM image in Fig. 5(a). The buried substrate steps lead to broadened steplike structures of height $\sim$0.7 Å and width $\sim$6 nm. Provided that the deformation areas do not overlap, the energy cost associated with this elastic deformation is proportional to the substrate step density, and will reduce the driving force for dewetting.

For a conservative (low) estimate of the reduction in free energy during dewetting, we neglect the lateral ripening of the film structures, assume vertical side walls and include only surfaces and interfaces parallel to the substrate surface. In this simplified 2D picture the energy change is

$$\Delta E_{\mathrm{dew}}=(\sigma_f+\sigma_{sf}-\sigma_s)\Delta A_W, \tag{1}$$

where σ_s and σ_f are the specific free surface energies for the substrate and the film, and σ_{sf} the specific free energy of the interface between substrate and film. ΔA_W denotes the change in area covered by silver, and is negative for the dewetting process. The $(\sigma_f+\sigma_{sf}-\sigma_s)$ value is not known exactly, but it must be positive for dewetting to occur. Though first attempts have been made to determine interface energies for selected model systems,[17,18] reliable values for interface energies are generally not available. If equilibrated films exhibit more than half truncated (i.e., flat) 3D crystals, as in our case of Ag/Si(111)$(\sqrt{3}\times\sqrt{3})$, $\sigma_s-\sigma_{sf}$ is positive but smaller than σ_f.[19] Using density-functional-theory calculations, Methfessel *et al.*[20] obtained $\sigma_f=76\ \mathrm{meV/Å^2}$ for the surface energy of Ag(111), yielding a dewetting energy on the order of mV—tens of $\mathrm{mV/Å^2}$.

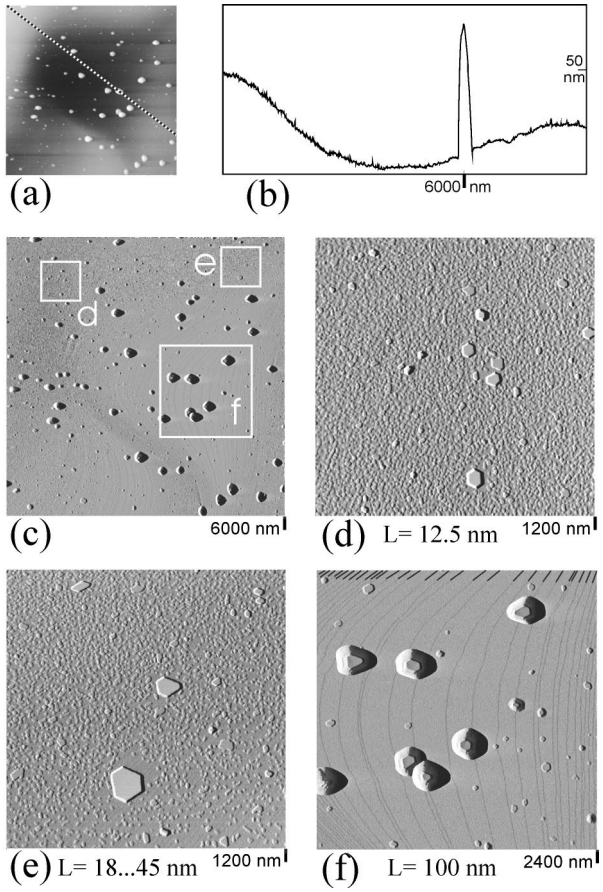

FIG. 4. A region with shallow curvature allows study of the substrate terrace width dependence of dewetting. A silver film was prepared by room temperature deposition of a 1 nm film, followed by a 450-min anneal at 275 °C. The state of agglomeration was frozen by quenching the sample to room temperature for the following STM measurements. (a) 6-μm overview of the investigated dimple (b) Height profile along the dotted line in (a) reveals variations in local curvature. The profile spike results from a 3D crystallite (c) Differentiated image of the 6μm overview in (a) with white boxes. (d)–(f) Locating regions with significantly different step densities. STM measurements of those regions then shown in (d). The average terrace width is $L=12.5$ nm. (e) $L=20$ nm and (f) $L=100$ nm. Note that the image contrast is adjusted at the top of (f) to highlight predeposition substrate step positions as dark lines. Larger crystallites form on wider substrate terraces, indicating that terraces facilitate dewetting.

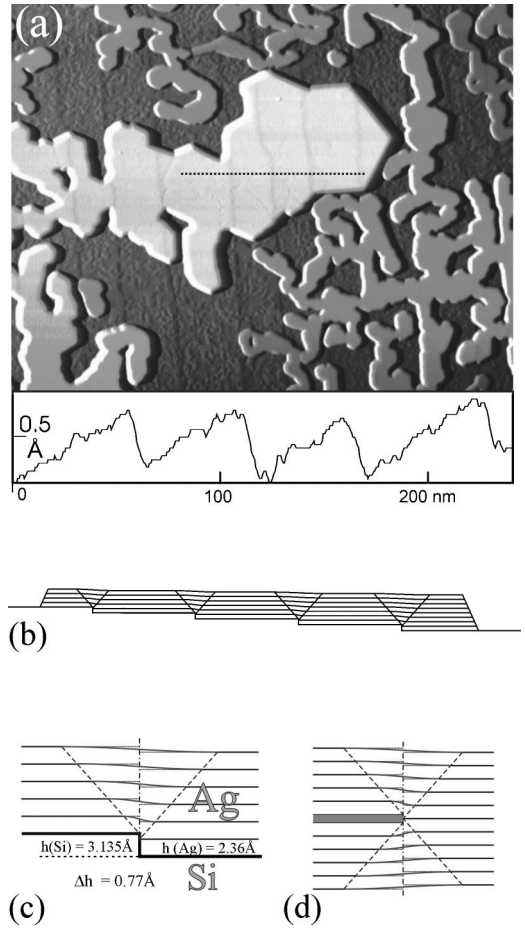

FIG. 5. The difference in step height between Si(111) and Ag(111) leads to a subtle but visible deformation of crystals that grow across Si steps. (a) 625×475 nm^2 STM topview of scan profile along dotted line. (b) and (c) Schematic side view of a distorted crystal. (d) Schematic drawing illustrating the analogy to the strain field of a step dislocation (see text). Silver film was prepared by room temperature deposition of a 1 nm film, followed by a 120-min anneal at 300 °C.

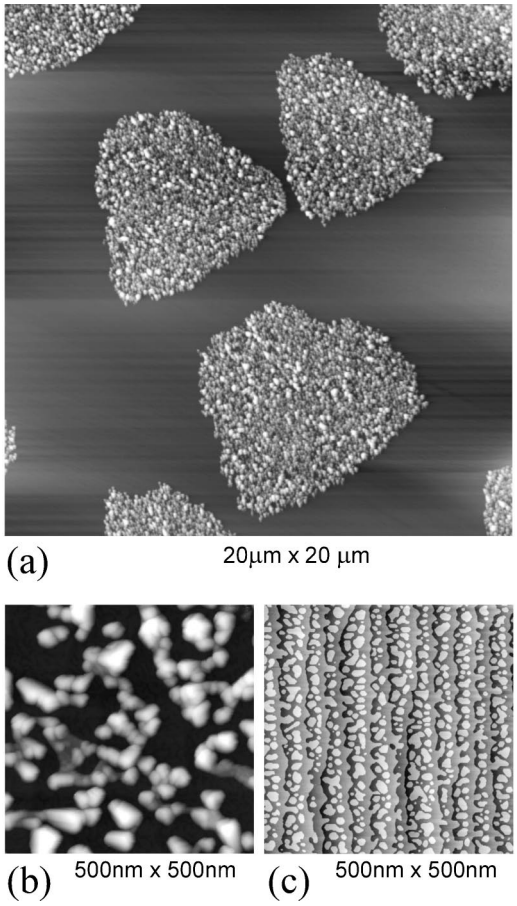

FIG. 6. (a) Large scale STM image of a surface created by room temperature deposition of 1-nm Ag onto a preprepared ($\sqrt{3}\times\sqrt{3}$)-$R30°$Ag/Si(111) substrate. This film morphology is the result of "spontaneous dewetting" at deposition temperature. (b) Zoom into one of the triangular cluster clouds reveals microcrystals of different orientations. (c) Bare ($\sqrt{3}\times\sqrt{3}$) substrate found between the triangular patches shows its characteristic two-level structure.

The energy gain ΔE_{dew} must be compared to the energy cost for the elastic deformation. Figures 5(c) and 5(d) illustrate the analogy to the strain field in the upper half space of a hypothetical step dislocation with a Burger's vector $b=2\Delta h=2(h_{\mathrm{Si}}-h_{\mathrm{Ag}})=1.54$ Å. Equating the energy per length of a buried step u_{bs} to half the energy for a step dislocation[21] yields

$$u_{bs}\approx u_{\mathrm{edgedis}}/2\approx \frac{\mu b^2}{8\pi(2-E/2\mu)}\ln(4R/b), \tag{2}$$

with the shear modulus μ, elasticity modulus E and the outer radius of the considered distortion field R. Since the width of the distorted stripe observed by STM equals roughly the thickness of the distorted crystal, we can conservatively use 3 nm as an approximation for R, although increasing the value of R up to a value of 100 nm will not change the qualitative conclusions below. Using the known values for $\mu(T=350\,°\mathrm{C})\approx25.5$ GPa and $E(T=350\,°\mathrm{C})\approx69.7$ GPa,[22] we arrive at $u_{bs}\approx0.103$ eV/Å. For the smallest average substrate terrace width studied, $L=12.5$ nm as in Fig. 4(b), this translates into an average distortion energy density per area of the crystallite of $\sigma_{\mathrm{disto}}=103$ meV/Å/125 Å $=0.8$ meV/Å^2. For this energy cost to impede the dewetting, the energy gain upon dewetting $\Delta E_{\mathrm{dew}}/\Delta A$ according to Eq. (1) cannot be larger than the strain energy per area of the crystallite:

$$\sigma_f+\sigma_{sf}-\sigma_s<0.8\ \mathrm{meV/Å^2}. \tag{3}$$

With the specific surface energy of ≈75 meV/Å^2 for Ag(111), we get

$$0.98\sigma_f<\sigma_s-\sigma_{sf}. \tag{4}$$

On the other hand, dewetting for step-free surfaces can only occur if $\sigma_s<\sigma_f+\sigma_{sf}$. Consequently, $\sigma_s-\sigma_{sf}$ would have to fall into the very narrow interval

$$0.98\sigma_f<\sigma_s-\sigma_{sf}<\sigma_f. \tag{5}$$

This constraint appears improbable. The observation that the growing crystallites do not avoid step crossings [e.g., Fig.

5(a)], but assume growth shapes that cross multiple steps, further suggests that step-induced strain is not the causal agent of the observed step-density dependence of dewetting. However, values for specific surface free energies are needed for a definitive conclusion on the role of elastic strain energy.

An alternate source of the dewetting sensitivity to step density is of kinetic origin. Substrate steps can be assumed to serve as diffusion barriers for Ag atoms and thus limit the feeding areas of growing crystals. Figure 3(h) seems to corroborate this effect: Crystallites develop relatively close to each other if they are separated by substrate steps. They apparently do not ''see'' each other and their depletion areas do not overlap. In the case of impenetrable steps, a crystal on a high step density substrate draws material from a narrow stripe, whereas a crystal on a wide terrace draws material from a larger area. As a consequence, material has to travel a longer path to grow a crystal of a given size on narrower substrate terraces.

Finally, the $(\sqrt{3}\times\sqrt{3})$-$R30°$Ag/Si(111) reconstruction that accompanies dewetting must be considered. To separate the influence of this reconstruction, we first prepared the $(\sqrt{3}\times\sqrt{3})$ phase by depositing 1 ML Ag at 350 °C. We then subjected the $(\sqrt{3}\times\sqrt{3})$-$R30°$Ag/Si(111) surface to room temperature deposition of a 1-nm Ag film. Even at room temperature, a remarkable film morphology [Fig. 6(a)] is observed. This 20×20-μm^2 survey image shows triangular patches consisting of ''clouds'' of a few thousand microcrystallites. After deposition of an additional 2–3-nm Ag these clouds of crystallites cover the entire surface (not shown). A zoom into such a patch [Fig. 6(b)] reveals $3d$ crystallites of typically 10 nm in height and residual bare substrate between these particles. X-ray diffraction experiments[8,23] suggest preferred orientations of Ag(110), (100), (111), and (311) parallel to the substrate. The area between these patches retains the $(\sqrt{3}\times\sqrt{3})$-$R30°$Ag/Si(111) under partial coverage by compact silver islands, as shown in Fig. 6(c).

We attribute this remarkable film morphology to spontaneous dewetting: At room temperature, the low mobility of Ag on Ag prevents the formation of the equilibrium configuration characterized by large 3D crystals. But the extremely high diffusion of Ag atoms on the $(\sqrt{3}\times\sqrt{3})$ surface combined with a strong driving force generated by a presumably very low surface energy of the $(\sqrt{3}\times\sqrt{3})$ phase initiates Ag agglomeration already at room temperature. The mesoscopic triangular shapes of these cluster clouds is an intriguing metastable geometry, which requires thermal activation to transform to large crystallites.

IV. CONCLUSIONS

These remarkable dewetted film structures demonstrate the importance of interface crystallinity in the dewetting of ultrathin (1 nm) solid state films. Dewetting is clearly a complex dynamical process that involves mass transfer across an evolving interface. For this Ag/Si system, the (extent of) $\sqrt{3}\times\sqrt{3}$-Ag reconstruction and the local density of crystallographic steps on the substrate impact dewetting dynamics and morphological evolution. On partially reconstructed substrates, patches of $\sqrt{3}\times\sqrt{3}$-Ag offer a higher silver mobility, providing a positive feedback (acceleration) in film dewetting. On fully reconstructed surfaces, this enhanced silver mobility leads to a spontaneous dewetting of ultra-thin silver films into a novel ''cluster cloud'' metastable structure.

Dewetting proceeds more readily on regions of low substrate step density. We have discussed possible thermodynamic and kinetic factors for this sensitivity to crystallographic steps. During the dewetting process, emerging crystallites frequently cross crystallographic steps, producing an elastic deformation of the emerging crystallites. We have provided a simple form to relate the energy gain in dewetting to the density of crystallographic steps. We have also discussed how steps reduce Ag-adatom mobility and thus limit dewetting rates, particularly at lower temperatures. To assess the relative contribution of elastic strain energy in the dewetting process, values for specific surface free energies are needed.

*Present address: Sandia National Laboratories, Livermore, California 94550, USA.

†Corresponding author. FAX: 301-314-9121. Electronic address: rrobey@wam.umd.edu

[1] E. Jiran and C. V. Thompson, J. Electron. Mater. **19**, 1153 (1990).

[2] U. Thiele, M. Mertig, and W. Pompe, Phys. Rev. Lett. **80**, 2869 (1998); P. Martin and F. Brochard-Wyart, *ibid.* **80**, 3296 (1998); R. Xie *et al.*, *ibid.* **81**, 1251 (1998).

[3] St. Tosch and H. Neddermeyer, Phys. Rev. Lett. **61**, 349 (1988).

[4] H. Neddermeyer, Crit. Rev. Solid State Mater. Sci. **16**, 309 (1990).

[5] F. Moresco, M. Rocca, T. Hildebrand, and M. Henzler, Surf. Sci. **463**, 22 (2000).

[6] J. A. Venables, J. Derrien, and A. P. Jansen, Surf. Sci. **95**, 411 (1980).

[7] D. Winau and R. Koch (unpublished).

[8] R. D. Aburano *et al.*, Phys. Rev. B **52**, 1839 (1995).

[9] A. W. Denier van der Gon and R. M. Tromp, Phys. Rev. Lett. **69**, 3519 (1992).

[10] A. Endo and S. Ino, Surf. Sci. **293**, 165 (1993).

[11] Y. Nakajima, G. Uchida, T. Nagao, and S. Hasegawa, Phys. Rev. B **54**, 14 134 (1996).

[12] X. Tong, Y. Sugiura, T. Nagao, T. Takami, S. Takeda, S. Ino, and S. Hasegawa, Surf. Sci. **408**, 146 (1998).

[13] W. Mullins, J. Appl. Phys. **30**, 77 (1959).

[14] A. Shibata, Y. Kimura, and K. Takayanagi, Surf. Sci. **303**, 161 (1994).

[15] T. Takahashi and S. Nakatani, Surf. Sci. **282**, 17 (1993), and references therein.

[16] M. Katayama, R. S. Williams, M. Kato, E. Nomura, and M. Aono, Phys. Rev. Lett. **66**, 2762 (1991).

[17] K. Højrup Hansen, T. Worren, S. Stempel, E. Lægsgaard, M. Bäumer, H.-J. Freund, F. Besenbacher, and I. Stensgaard, Phys. Rev. Lett. **83**, 4120 (1999).

[18] A. Bogicevic and D. R. Jennison, Phys. Rev. Lett. **82**, 4050 (1999).

[19] R. Kaischew, Bull. Acad. Sci. Bulg., Ser. Phys. **2**, 191 (1951).
[20] M. Methfessel, D. Hennig, and M. Scheffler, Phys. Rev. B **46**, 4816 (1992).
[21] J. P. Hirthe and J. Lothe, *Theory of Dislocations* (Wiley, New York, 1982).
[22] F. Kohlrausch, *Praktische Physik* (Teubner, Stuttgart, 1986), Vol. 3, p. 40.
[23] K. Akimoto, M. Lijadi, S. Ito, and A. Ichimiya, Surf. Rev. Lett. **5**, 719 (1998).